Science Robotics
AAAS

Supplementary Materials for

A minimally invasive robotic spinal surgical system for anterior lumbar nerve decompression

Qingxiang Zhao *et al.*

Corresponding author: Jiancheng Zeng, tomzeng5@163.com; Kang Li, likang@wchscu.cn

Sci. Robot. **11**, eadu0590 (2026)
DOI: 10.1126/scirobotics.adu0590

The PDF file includes:

Other Supplementary Material for this manuscript includes the following:

Supplementary Results

Table S1. Basic Tube Design Parameters (Unit: mm).

	Proximal Segment		Distal Segment	
	Outer Tube	Inner Tube	Outer Tube	Inner Tube
OD	2	1.7	1.4	1.1
ID	1.8	1.5	1.2	0.9
Tenon-mortise Section Length	15	15	18	18
Passive Compliant Section Length (Figure S9-③)	0	0	48	48
Rigid Section Length (Figure S9-①)	124	118	80	76
Passive Compliant Section Length (Figure S9-⑤)	73	84	107	114
Rigid Section Length (Figure S9-②)	256	312	376	434

Table S2. Boundary values of tenon-mortise slits design parameters. 'Constant' means the parameter is predefined.

Variable	Minimum	Maximum	Variable	Minimum	Maximum
L (mm)	Constant		N (integer)	1	1000
Tubes OD (mm)	Constant		n (integer)	1	1000
Tubes ID (mm)	Constant		d_s	0.03	0.06
β (°)	15	50	d_h	0.25	0.3
l_s (mm)	0.1	0.7	θ_s	45	75
d_g (mm)	0.3	0.6			

Table S3. Design parameters of slits for the four tubes.

	Proximal Segment		Distal Segment	
Design Parameter	Outer Tube	Inner Tube	Outer Tube	Inner Tube
β (rad)	0.35	0.36	0.35	0.35
l_s (mm)	0.59	0.56	0.44	0.49
d_g (mm)	0.51	0.31	0.50	0.50
N	27	41	34	32
n	4	4	6	3
d_s (mm)	0.036	0.054	0.03	0.06
d_h (mm)	0.26	0.26	0.28	0.31
θ_s (rad)	1.02	1.03	0.87	1.05

Table S4. Tip Deviation for the single proximal segment and the dual-segment arm under various actuation settings and loads (Unit: mm).

Push Distance Applied	Only Proximal Segment		Dual Segment	
on the Inner Tube	20g Load	50g Load	20g Load	50g Load
1 mm	2.46	3.51	8.92	12.6
2 mm	2.31	2.42	9.56	13.5
3 mm	1.64	2.12	11.3	16.8

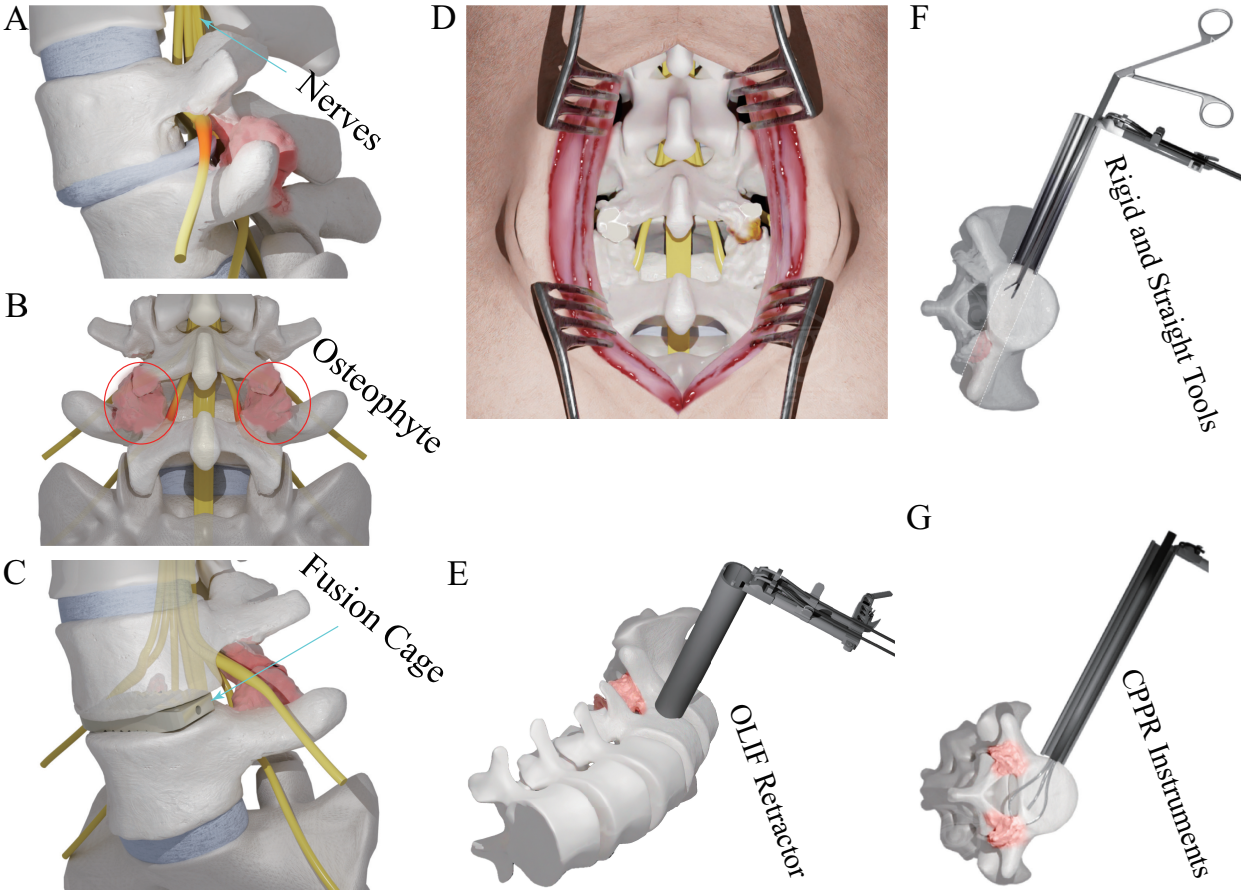

Figure S1. **Basics of lumbar degenerative diseases, existing surgical approach and our robot-assisted treatment method.** (A) Degenerative spinal structures compress lumbar nerves, so patients feel pain in the lower back and legs. (B) Rear view of spine. Osteophyte at the articular joint processes compressed nerves. (C) Implant a fusion cage in intervertebral disc to expand space for the nerves and restore stability of spine. (D) Posterior method to resect the degenerative structures, which needs an incision port of around 8 cm in length, and intraoperative blood loss is around 300 to 500 mL. (E) OLIF approach. Build a corridor using OLIF retractor to enable instruments to reach the front side of vertebrate. (F) Rigid and straight surgical tools enter the space of intervertebral disc but the surgeon has limited operation space and occluded visual field, leading to incomplete and indirect decompression outcome. (G) Use CPPR-based dexterous instruments to pass through the intervertebral disc and completely resect the degenerative structures at the posterior and anterior areas of spine.

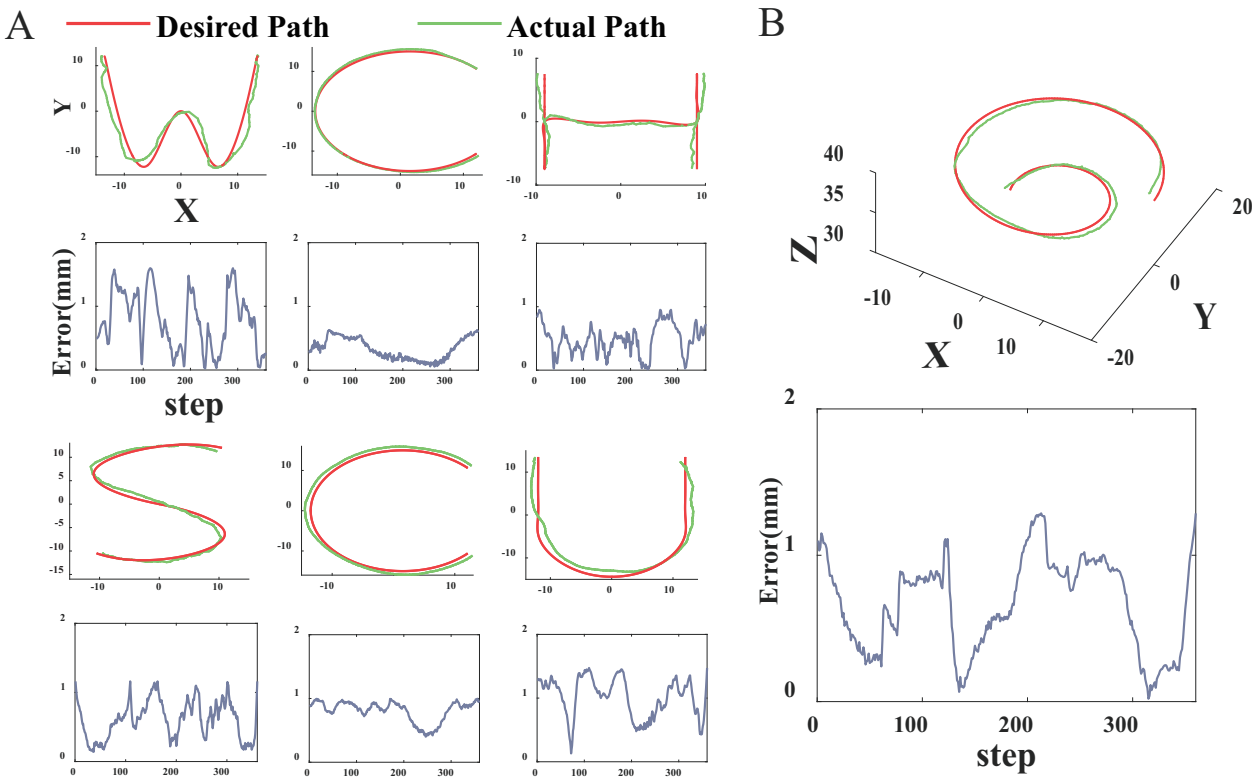

Figure S2. **Path-following task and tip position error. The velocity of the tip marker is around 9 mm/s. Lower velocity will contribute to higher accuracy.** (A) 2D path following results and error. (B) 3D path following result and error.

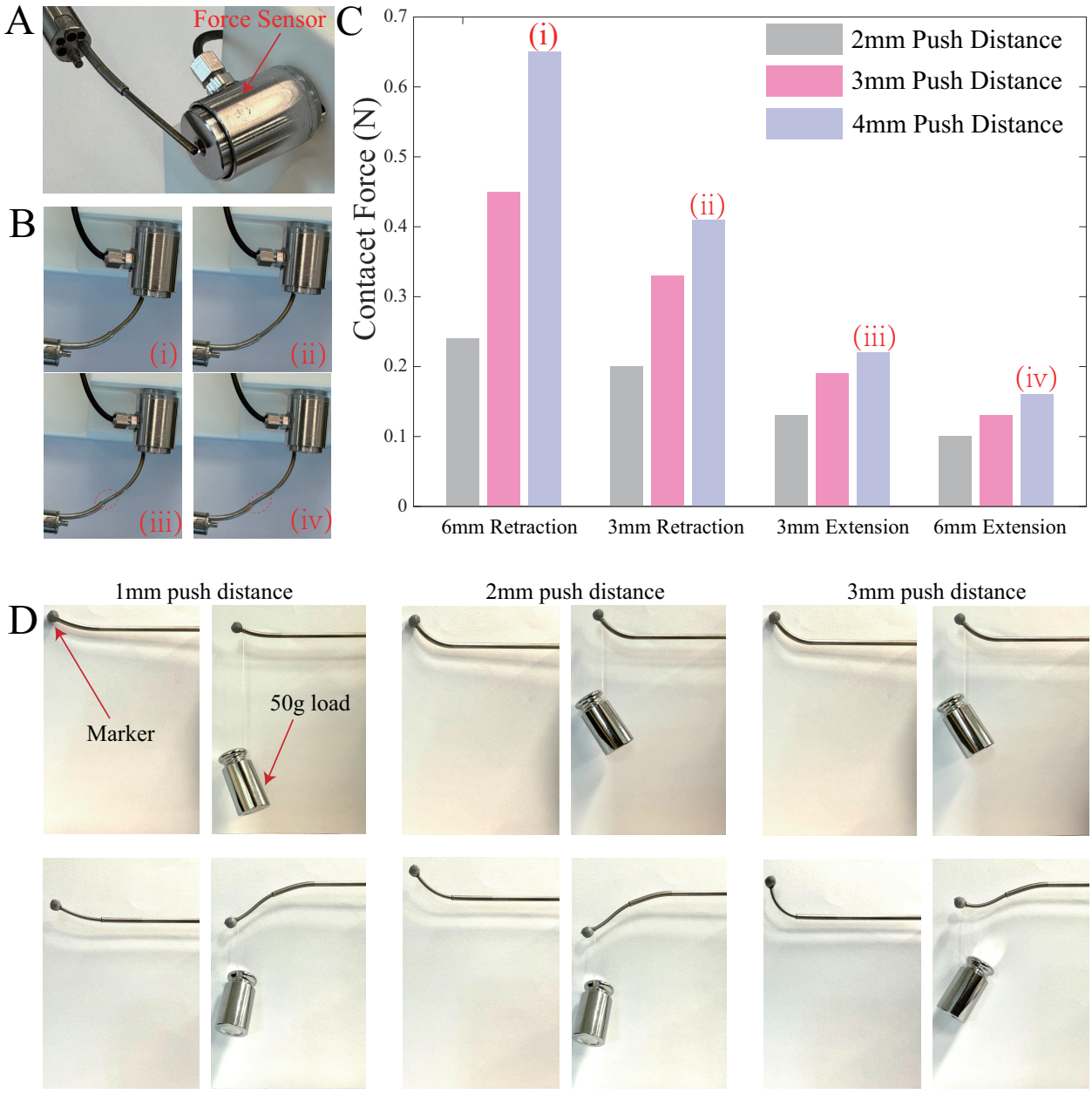

Figure S3. **Stiffness tests on the whole arm.** (A) Experiment setup for testing the stiffness of the dual-segment robot arm. (B) Key snapshots of one dual-segment robot arm interacting with the force sensor. While the passive compliant section of the distal segment extends from the proximal segment, larger push distance acting on the inner tube generates more notable deformation (highlighted in red dashed ellipse). In load-free scenario, the passive compliant section is straight, but it also deforms to adapt with obstacles, which is friendly to manipulate delicate tissues, such as nerves. (C) Snapshots of the robot arm in load-free and with-load scenarios. The position deviation between the two scenarios shows the ability of withstanding payload.

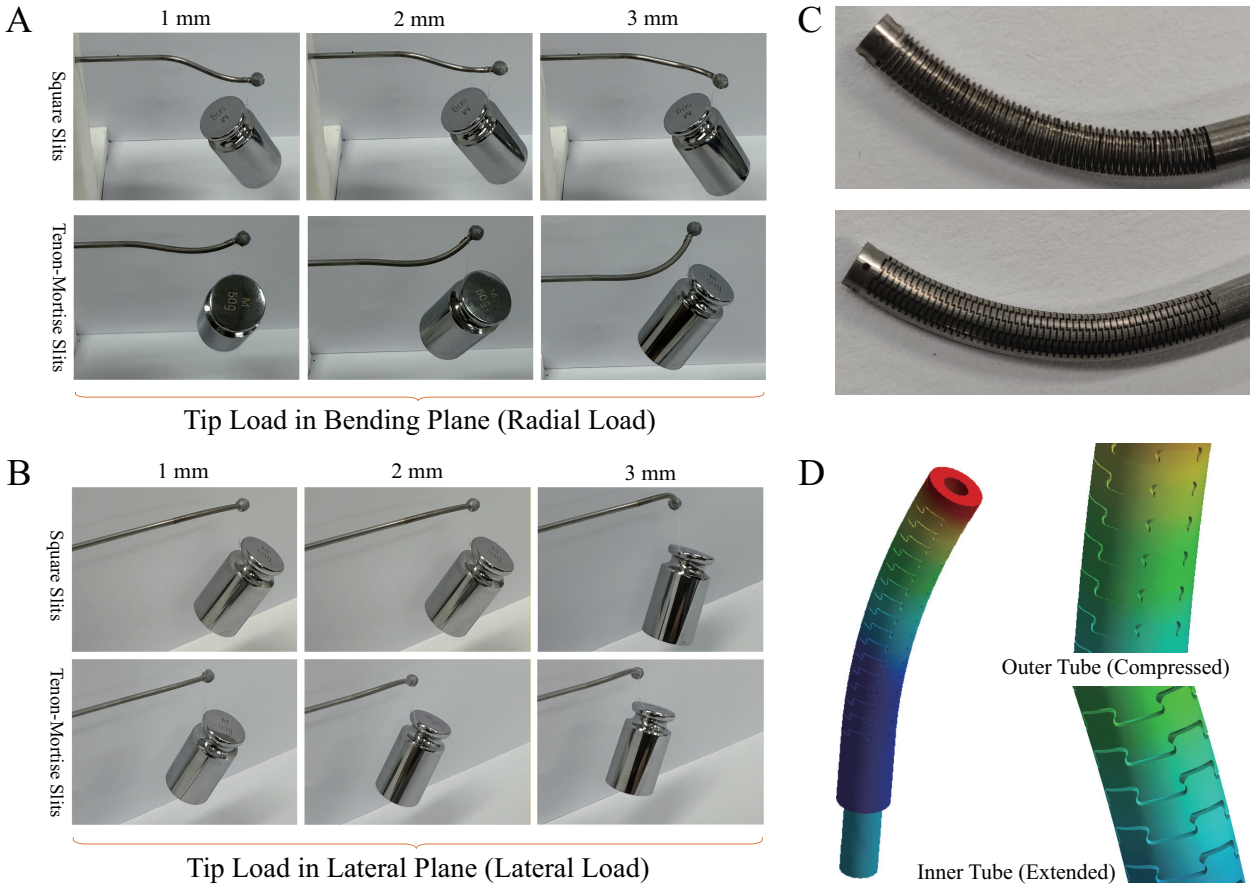

Figure S4. **Stiffness comparison between tenon-mortise and square-slit CPPR arms (identical dimensions except slit type).** (A) One load of 50 g was hung at the tip to generate radial load. (B) One load of 50 g was hung to generate lateral load. (C) Comparison of square slits and tenon-mortise slit in bending shape, and the tenons and mortises interlock together. While for the square slits design, much of the area is vacated. (D) FEM analysis results about the tenon-mortise slits design, and the slits on both the inner tube and the outer tube simultaneously interlock together.

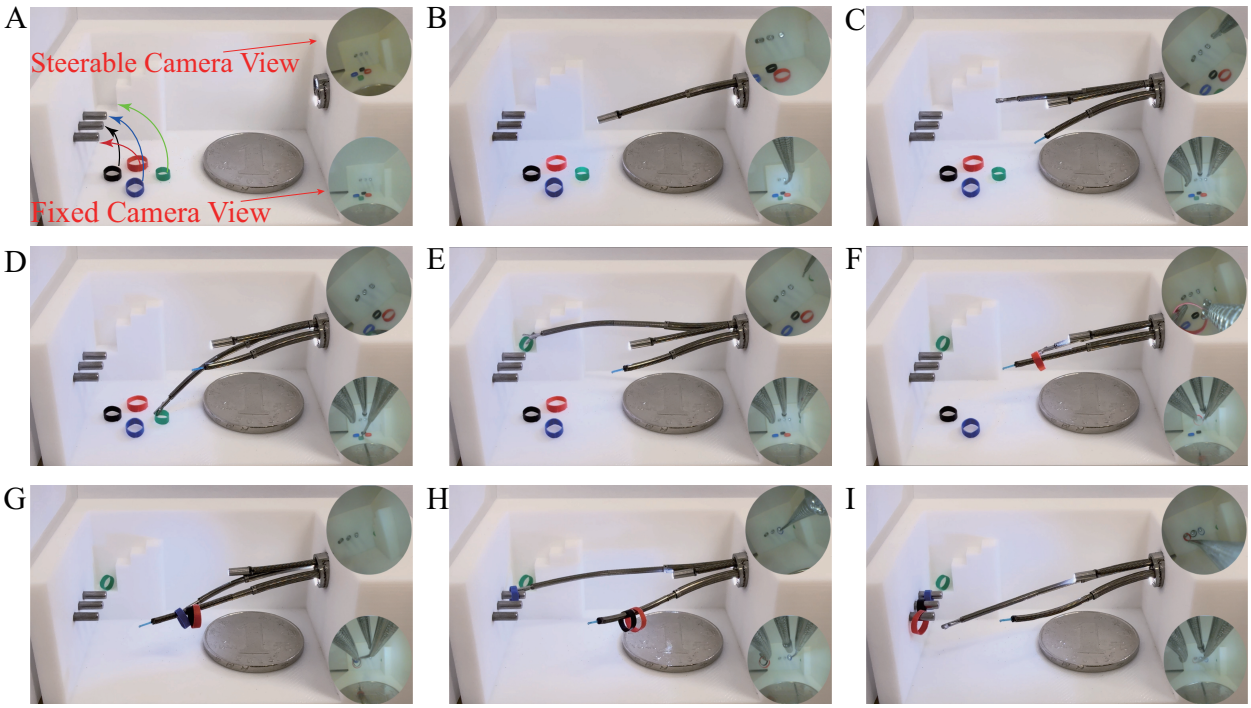

Figure S5. **Key snapshots illustrating multi-arm coordination.** (A) The three robotic arms are commanded to collect and place four rubber rings to specific targets sequentially under endoscopic view as guidance. A coin is placed to show the narrow task space to provide a scale reference. (B) Extension of the steerable camera arm. (C) The three steerable instruments all extend from the trocar and reach the task space. (D) The gripper arm is picking up the green rubber ring. (E) Placement of the green rubber ring into a $3 \times 3 \times 3$ mm semi-closed corner. (F) Retrieval of the red rubber ring and its hanging on the laser optical fiber arm. (G) Completion of ring collection and hanging on the laser arm. (H) Sequential retrieval of the rubber rings for placement onto three target columns. (I) Successful placement of all rubber rings at their designated targets.

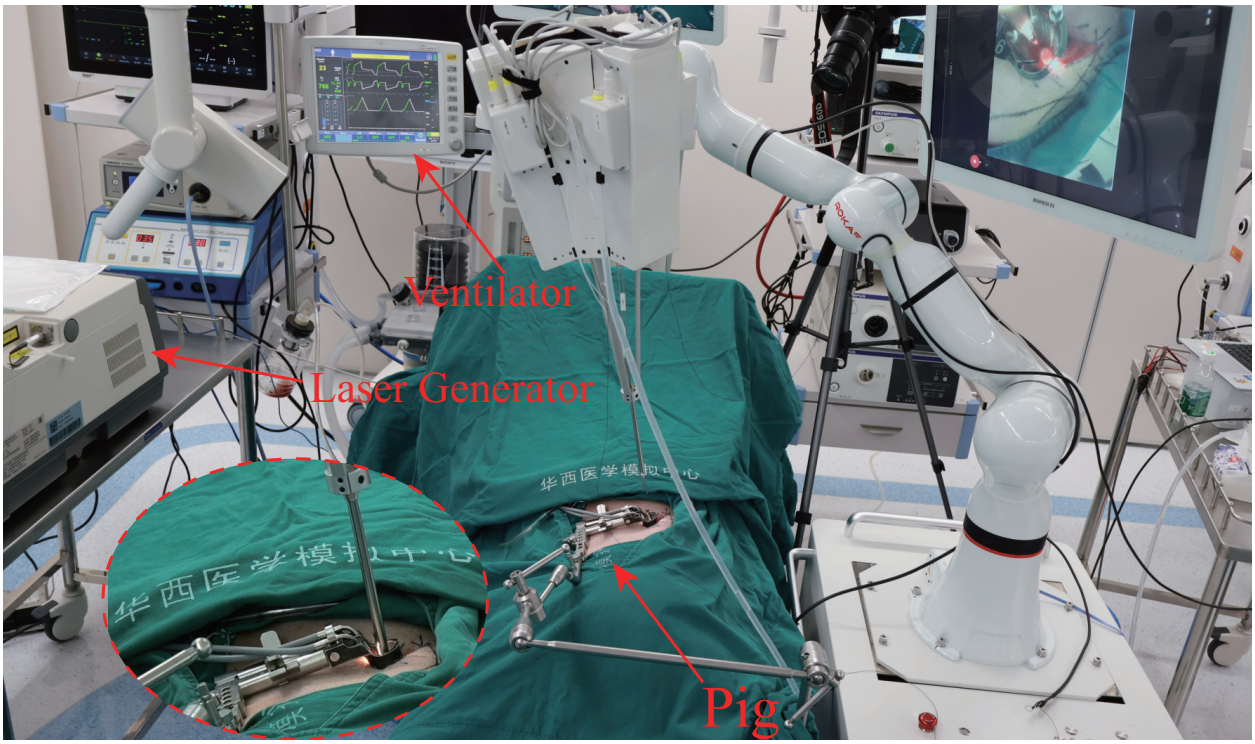

Figure S6. **In vivo animal experiment setup.** A standard OLIF retractor was employed to build the corridor. Ventilator always monitored the key parameters of the pig. The robot system was arranged beside the operating bed, and the pig was in right body position. Thulium laser generator provided energy for hemostasis and for resection.

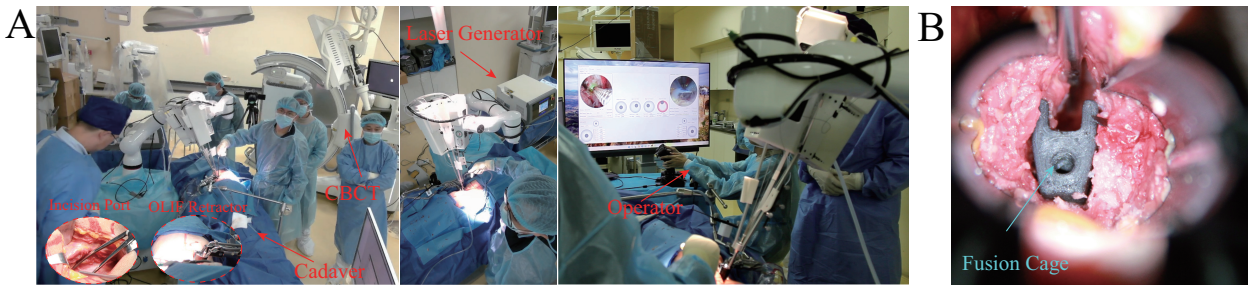

Figure S7. **Human cadaver tests setup.** (A) Operation room setting. The CBCT collected fluoroscopic images to confirm the surgical targets. (B) Implant a fusion cage at the vacated intervertebral disc space after decompression procedure.

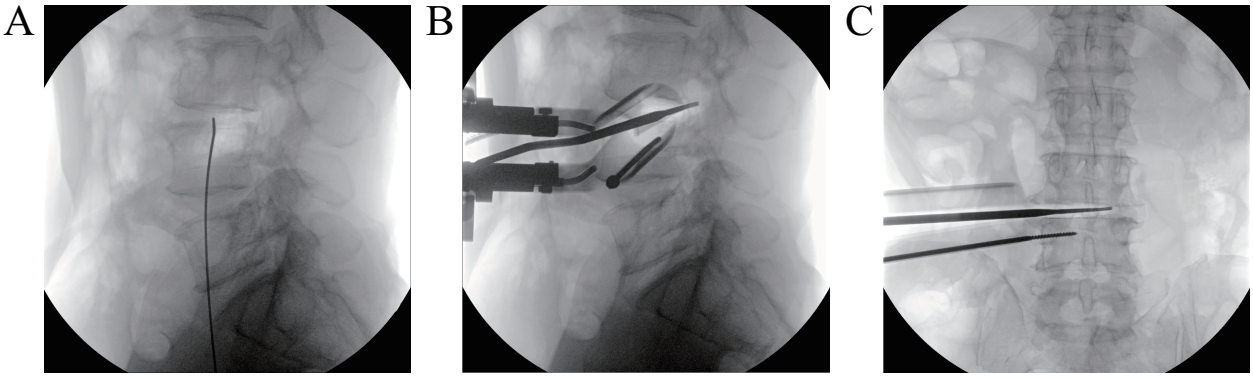

Figure S8. **Fluoroscopic images for confirming the surgical site.** (A) Lateral view of spine after inserting a guidewire at the target intervertebral disc. (B) Lateral view of spine after building the corridor by the retractor. (C) Posterior view of spine with a straight dissector inserted.

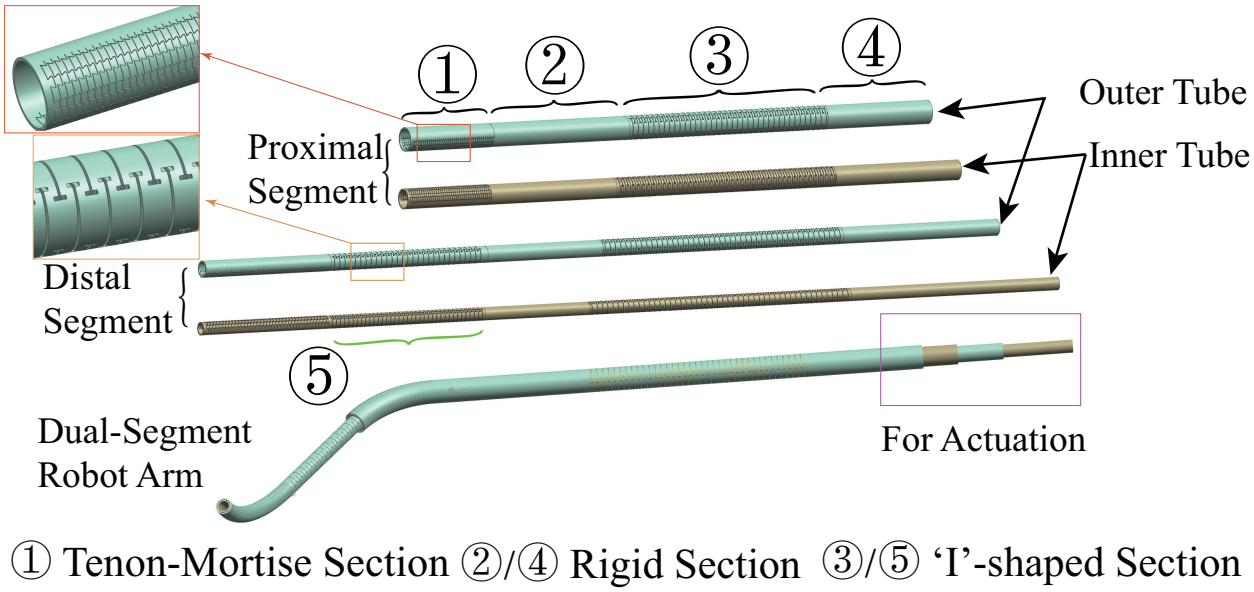

Figure S9. **Basic illustration of four hollow steel tubes forming one dual-segment robot arm.** Each segment consists of a pair of tubes that are fixed at the tip. For the proximal segment, each tube has 4 sections from the tip to the end, including tenon-mortise section, rigid section, 'I'-shaped section and actuation section. For the distal segment, it has an additional 'I'-shaped section to passively adapt with the shape of the proximal segment. At the end, the rigid section was designed for actuation (labeled by pink box).

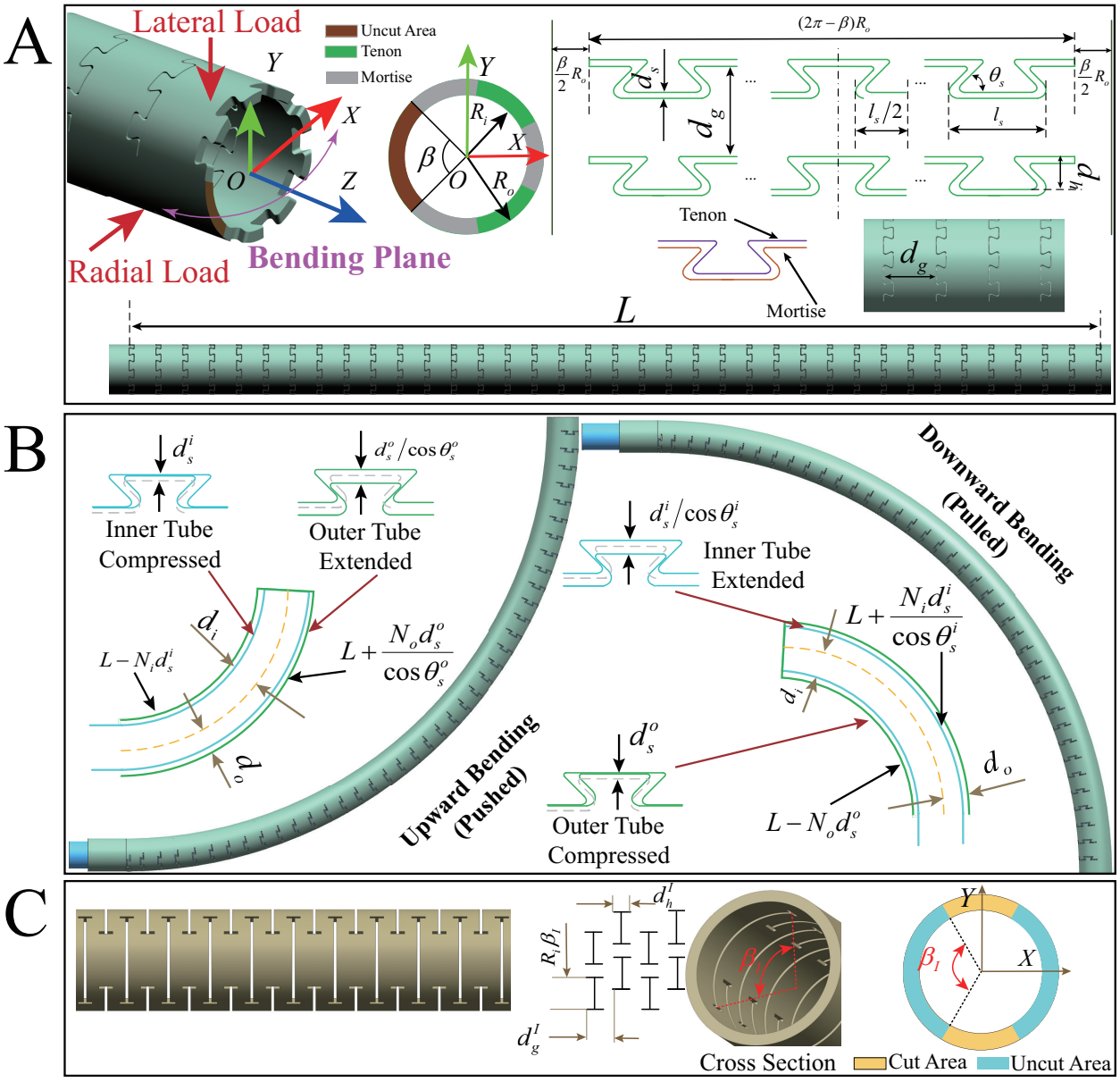

Figure S10. **Detailed design parameters of one segment.** (A) Parameters of tenon-mortise slits. (B) For one bendable segment, pushing or pulling the inner tube generates 2D arc bending at the patterned section. The tenon-mortise slits on the two tubes are both required to interlock together simultaneously, enhancing rigidity. (C) Parameters of the 'I'-shaped section.

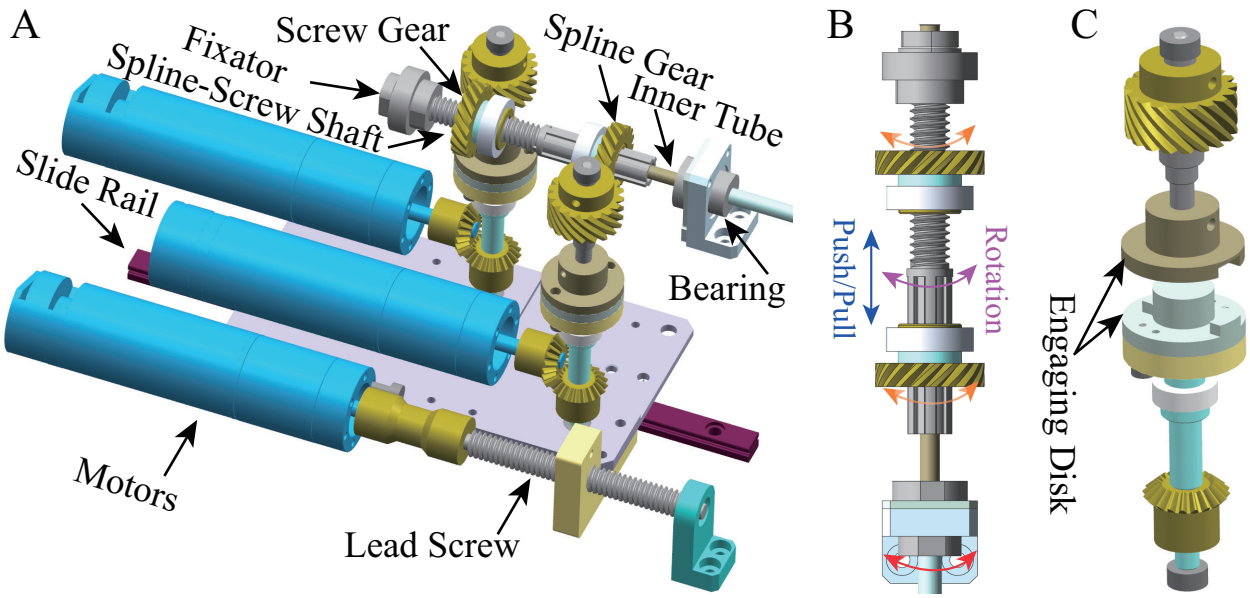

Figure S11. **key actuation module for a single segment.** (A) The outer tube is fixed on a bearing, and the inner tube is fixed on a spline-screw shaft. One DC motor rotates a lead screw to realize translation of the whole module. (B) Two gears (a spline gear and a screw gear) are respectively assembled on the shaft. Once the two gears rotate at an equal velocity (labeled by orange arrows), the shaft rotates accordingly (purple arrow). When the screw gear rotates and the spline gear keeps static, translational motion is achieved and the inner tube is being pushed or pulled (blue arrow). Two pairs of helical gear transmit motion from the motors. (C) For quick release/assembly, we designed engaging disk structures on the instrument component and the actuation component. The angle gear connects with a DC motor.

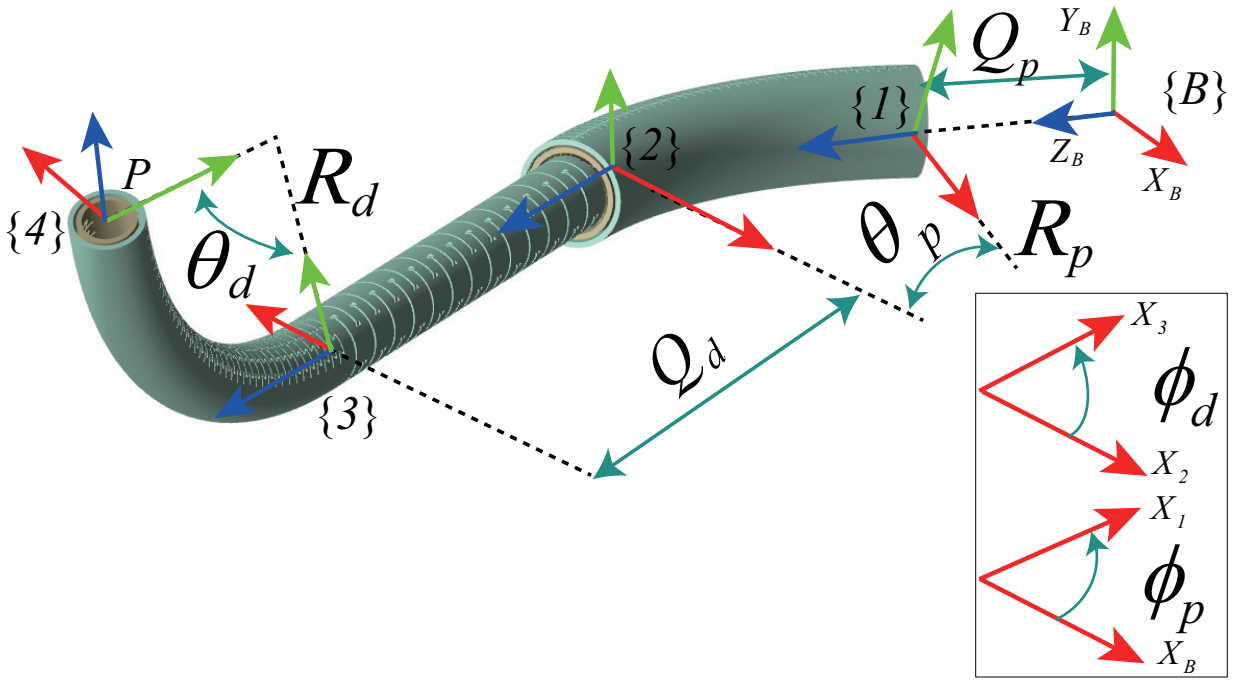

Figure S12. **Kinematics modeling of the dual-segment robot shape.** For a robot arm, the shape of each segment is assumed as an arch, so the robot tip position with respective to the base frame can be accordingly solved via the shape parameters. Translation, rotation and bending DoFs are expressed by Q, ϕ and θ, respectively.

Table S1. Detailed Tube Design Parameters (Unit: mm).

Table S2. Boundary values of tenon-mortise slits design parameters. 'Constant' means the parameter is predefined.

Table S3. Design parameters of slits for the four tubes.

Table S4. Tip Deviation for the single proximal segment and the dual-segment arm under various actuation settings and loads (Unit: mm).

Movie S1. Basics of the robot system. This video shows the process of assembling one instrument component on the actuation component, which only needs around 20s for quick exchange instruments in surgery. In addition, the motion of each instrument is shown, including motion of any single robot arm and their coordination.

Movie S2. Performance of a single robot arm. A dual-segment robot arm follows various paths, and the capability of carry weight is shown in this video.

Movie S3. Arm-Arm coordination and animation about key decompression procedures. Dexterous slender instruments collect small rubber rings and place them sequentially to targets, and the endoscopic camera views are the only visual feedback for the operator. During surgery, the gripper functions to dissect and grip tissues, and the laser optical fiber arm cauterizes veins to stop bleeding and resect degenerative spinal structures.

Movie S4. In vivo animal experiment. Robotic instruments incise the intervertebral disc of a porcine spine and reached the posterior area.

Movie S5. Human cadaver tests. Videos from the endoscopic cameras to show the key procedures of decompression in a cadaver.